

Qualification Tests of the R11410-21 Photomultiplier Tubes for the XENON1T Detector

P. Barrow,^a L. Baudis,^a D. Cichon,^b M. Danisch,^b D. Franco,^a F. Kaether,^b A. Kish,^a M. Lindner,^b T. Marrodán Undagoitia,^b D. Mayani,^{a,*} L. Rauch,^{b,*} Y. Wei,^a J. Wulf^a

^a*Physik Institut, Universität Zürich,
8057 Zürich, Switzerland*

^b*Max-Planck-Institut für Kernphysik
69117 Heidelberg, Germany*

E-mail: dmayani@physik.uzh.ch, rauch@mpi-hd.mpg.de

ABSTRACT: The Hamamatsu R11410-21 photomultiplier tube is the photodetector of choice for the XENON1T dual-phase time projection chamber. The device has been optimized for a very low intrinsic radioactivity, a high quantum efficiency and a high sensitivity to single photon detection. A total of 248 tubes are currently operated in XENON1T, selected out of 321 tested units. In this article the procedures implemented to evaluate the large number of tubes prior to their installation in XENON1T are described. The parameter distributions for all tested tubes are shown, with an emphasis on those selected for XENON1T, of which the impact on the detector performance is discussed. All photomultipliers have been tested in a nitrogen atmosphere at cryogenic temperatures, with a subset of the tubes being tested in gaseous and liquid xenon, simulating their operating conditions in the dark matter detector. The performance and evaluation of the tubes in the different environments is reported and the criteria for rejection of PMTs are outlined and quantified.

KEYWORDS: Photomultiplier; photosensors; dark matter; XENON1T.

*Corresponding authors.

Contents

1	Introduction	1
2	Testing procedure and experimental setups	2
2.1	General testing facility	3
2.2	Xenon testing facility	4
3	PMT parameter measurements and distributions	5
3.1	Quantum efficiency	5
3.2	Gain distribution	6
3.3	Single photoelectron resolution and peak-to-valley ratio	7
3.4	Transit time measurement	8
3.5	Dark count rates	9
4	Detection of light emitting PMTs	10
5	Measurements in gaseous and liquid xenon	12
5.1	Dark count rate stability	12
5.2	Gain evolution	13
6	Study of afterpulses and leak identification	13
6.1	Ion identification through afterpulse timing	14
6.2	Afterpulse analysis and leak diagnosis	16
7	Summary	18

1 Introduction

The direct detection of dark matter particles scattering off target nuclei is one of the most sought-after measurements in modern physics. In the last decade, dual-phase time projection chambers (TPC), operated with liquified xenon (LXe), have reached the highest sensitivity for Weakly Interacting Massive Particle (WIMP) interactions above masses of $5 \text{ GeV}/c^2$ [1][2]. The XENON1T experiment [3] is designed to further improve this sensitivity, searching for WIMPs through their scattering off xenon nuclei. The expected recoil energies, in the order of a few keV, induce transitions in various molecular states of xenon that result in the scintillation of vacuum ultraviolet (VUV) photons with a wavelength of 178 nm [4]. In addition, particle recoils produce free electrons that are drifted and extracted from the liquid by an applied electric field to be subsequently amplified in the gaseous xenon volume. Recombinations of these amplified electron showers in the gas produce additional photons via electroluminescence that enable the measurement of a secondary signal. It becomes evident that a successful detection of particle interactions in liquid xenon

can only be achieved by an efficient detection of VUV photons. To reach the highest possible sensitivities to dark matter interactions, the photomultiplier tubes (PMTs) are required to have a high photon detection efficiency (quantum efficiency), ultra low radioactivity levels [5] and stable long-term performance at operating temperatures of $-100\text{ }^{\circ}\text{C}$.

In this article, the evaluation tests of 321 Hamamatsu R11410-21 PMTs are described. The selection criteria for the final 248 tubes for XENON1T are discussed, based on characteristic parameters such as the dark count rate, quantum efficiency, afterpulse rate, light emission, long-term stability, peak-to-valley ratio and single photoelectron (SPE) resolution. The general testing procedure and experimental facilities are introduced in section 2. The distributions of measured and derived PMT parameters are shown in section 3. Section 4 describes the emission of light by some of the tested PMTs, being one of the major rejection criteria. Dedicated measurements of the long-term stability in cryogenic xenon environments are presented in section 5. Here the evolution of the dark count rates and gains is reported. Section 6 describes a detailed study of the afterpulse spectra and the methods used to determine the presence of leaks in faulty PMTs by identification of residual gas molecules. The conclusions of this article are summarized in section 7.

Complementary studies of earlier versions of the R11410 phototube have been reported in [6][7].

2 Testing procedure and experimental setups

The Hamamatsu Photonics R11410-21 is a circular-window PMT with a 3-inch diameter produced specifically for low background applications, such as dark matter detectors. The final version of the tube is a result of several iterations of construction material selection for the reduction of the total radioactivity of the device. After production and shipment, each PMT has been screened for its intrinsic radioactivity with high-purity germanium detectors [8][9][10][11]. The average levels measured per PMT are lower than 0.4 mBq/cm^2 for ^{238}U and $0.012(3)\text{ mBq/cm}^2$ for ^{228}Th [5].

After screening, every PMT is tested in air at room temperature and in nitrogen gas at around $-100\text{ }^{\circ}\text{C}$, close to the liquid xenon temperature (which will also be referred to as “cold”). The testing setups used for all PMTs are described in section 2.1. These overall tests verify the agreement of various PMT parameters with the production specifications, such as the gain, transit time, dark count and afterpulse rates. In addition, a PMT characterization is performed, including the voltage dependency of the gain, the signal resolution and the afterpulse spectrum. Every PMT is cooled down a minimum of 2 times to evaluate its performance at cryogenic temperatures and test its level of light emission (some PMTs have shown a quantifiable emission of photons, which will be described in section 4).

A subset of the tubes has been selected to be further tested in gaseous and liquid xenon with the setup described in section 2.2. There, the PMTs are operated over longer periods of time, from a couple of weeks to several months, and the dark count rate and gain evolution are measured. Dedicated measurements are performed to study the afterpulse spectra after each cool down.

The voltage divider bases for the PMTs in these setups have the same design as those used in XENON1T, with a negative bias operation. The divider has been developed for an optimal PMT performance in terms of gain and linearity, as well as the restrictions in heat dissipation and radioactivity for a LXe dark matter detector [12].

2.1 General testing facility

The first experimental setup is a dark room designed to test 12 PMTs simultaneously at room temperature. Installed within a large Faraday cage, which provides a low-noise environment, each PMT is mounted in a compartment equipped with an optical fiber connected to an LED emitting at 380 nm. The LED is controlled via a custom VME board providing a narrow pulse width of 1.4 ns, necessary for precision timing measurements. This setup allows to perform a high voltage scan to determine the gain values, measure the single photoelectron response, the afterpulse spectrum and transit time spread of the PMTs [13].

The second setup consists of a cooling tank designed for stable operation at cryogenic temperatures. The inner volume is filled with nitrogen vapor and cooled by a copper coil at the top, which is constantly flushed with liquid nitrogen. Inside the tank, two parallel arrays of 6 PMTs each are operated with the tube windows of one array facing those of the other. The temperature is measured at several positions with PT100 sensors to ensure a stable temperature within a few degrees during the measurements lasting for several hours. A schematic of this setup is shown in figure 1.

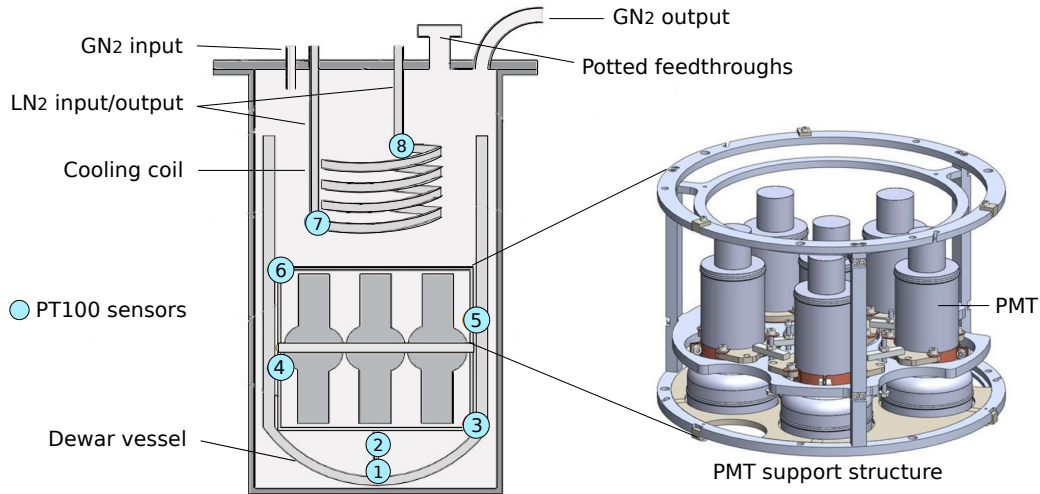


Figure 1. Schematic of the PMT setup for cryogenic temperature testing in nitrogen gas stabilized at -100°C . Two arrays of 6 PMTs each (left figure) are inserted into the dewar with the PMT windows facing the opposite array. Several PT100 sensors allow to measure and control the inner temperature within a few degrees by regulating the flow of the nitrogen through the coil.

Each PMT signal is initially amplified by a factor of 10 and sent to a fan out. The signal is split and read out by a charge-to-digital converter (QDC). The signal is amplified once more by a factor 10 and sent to a discriminator to be subsequently analyzed by a scaler and a time-to-digital converter (TDC). The TDC has a maximal time span of $1.2\mu\text{s}$ with a time resolution of 0.3 ns. The outputs of the QDC, TDC and scaler are read out by a computer where the time information of the LED trigger is also available to, for example, control the QDC time-integration window. Detailed information can be found in [13].

2.2 Xenon testing facility

A subset of the PMTs (around 15 %) has been tested in a third experimental setup where they are operated in both gaseous and liquid xenon for periods ranging from a couple of weeks up to several months. These tests evaluate the performance and stability of the PMTs in the same conditions in which they are operated in the XENON1T dual-phase TPC, with the top array in gas and the bottom array in liquid.

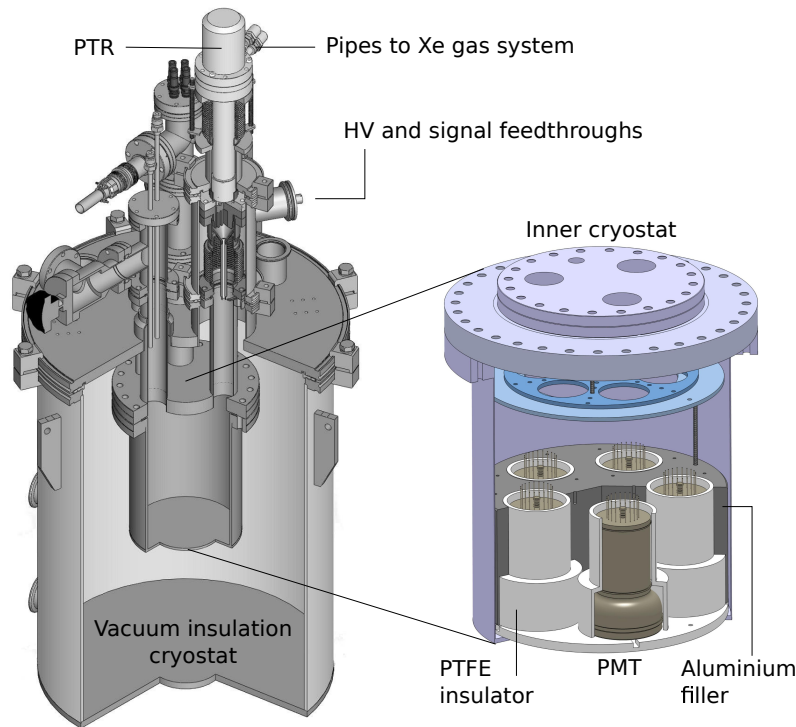


Figure 2. Schematic of the testing facility for PMTs in both gaseous and liquid xenon environments. The inner cryostat houses up to 5 PMTs simultaneously. The aluminium filler reduces the amount of LXe required to cover the PMTs, while the PTFE covers insulate the metallic bodies. A larger cryostat provides the inner chamber with vacuum insulation during cryogenic operation.

The xenon testing facility consists of a double-walled vacuum-insulated cryostat housing up to 5 R11410 PMTs simultaneously. Figure 2 shows a schematic of the experimental setup. The inner cryostat contains 5 PMTs facing a polytetrafluoroethylene (PTFE) reflector. A circular space is provided below each PMT and linked to all others through a central volume of the reflector. A PTFE insulator separates the PMTs from the aluminium filler, used to reduce the amount of LXe required to cover the sensors. Two temperature sensors have been installed, one at the bottom next to the PMT windows and another above the filler at the height of the PMT pins. A blue LED (470 nm wavelength) is installed in the common volume of the PTFE reflector between the PMTs. In addition, up to 4 optical fibers are placed close to that same location, coupled to a blue LED located outside of the cryogenic system.

Gaseous and liquid xenon can be filled into the system, surrounding the PMTs through the

space between the bodies and the PTFE covers. The cooling power for xenon liquefaction is provided by a pulse tube refrigerator (PTR). Xenon is circulated through a dedicated gas system that controls the flow into and out of the cryogenic chamber. It is equipped with a heated getter to remove impurities.

The setup features the same 2.1 mm PTFE coaxial cables and single wire Kapton cables currently used for signal and HV in the PMT arrays of XENON1T, respectively. Custom connectors designed with low radioactivity materials specifically for XENON1T have also been used and tested here [14]. Potted feedthroughs link the cabling of the PMTs inside the vessel to the external electronics for data acquisition. The signals go through a ten-fold amplifier and a fan out. For counting measurements, such as dark count rates, a discriminator is used along with a multi-channel scaler. Signals are digitized with a flash ADC and analyzed with a dedicated processing software.

3 PMT parameter measurements and distributions

This section summarizes the results of the tests performed on 321 PMTs, of which 248 were selected for XENON1T. These measurements have been taken in the testing facility described in 2.1, with every PMT following the same procedure in order to have comparable results. The derived parameters for the PMT characterization are briefly defined and their implications for a dark matter search are outlined.

3.1 Quantum efficiency

To enable a low energy threshold of the XENON1T experiment a high light collection efficiency is required and, hence, a high average quantum efficiency (QE) of the PMTs. The tubes have been pre-selected by Hamamatsu with a QE higher than 28%, as contracted.

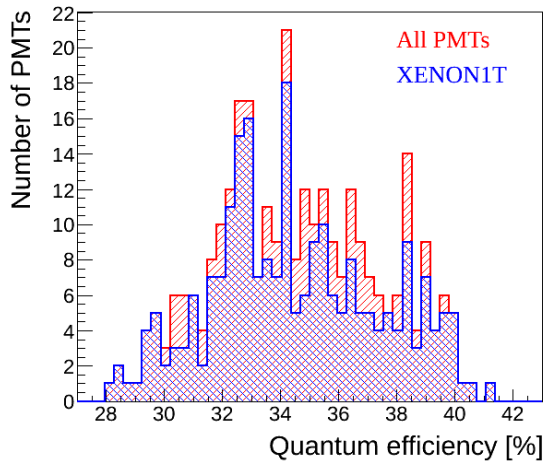


Figure 3. Distribution of the quantum efficiency for all tested PMTs (red) and the 248 selected for XENON1T (blue). The values correspond to those provided by Hamamatsu. The company pre-selected the PMTs with a QE higher than 28%, as contracted. Both distributions show an average around 34.5 % and a standard deviation of 2.8 %.

The QE distributions for all PMTs and the XENON1T selection, as measured by Hamamatsu, are shown in figure 3. The average QE is considerably high, with a mean value of approximately 34.5 % and a standard deviation of 2.8 % for both distributions. A study of the spatial distribution of the photon detection sensitivity can be found in [15], while the temperature and wavelength dependence of the QE has been studied in [16].

3.2 Gain distribution

The PMT response to a light source inducing single photoelectrons can be quantified by measuring the charge spectrum as seen in figure 4 (left).

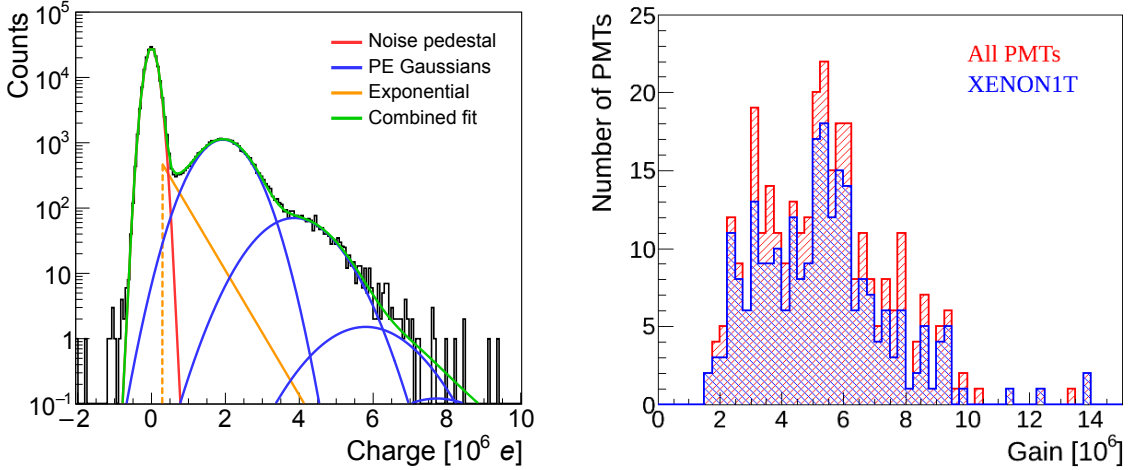


Figure 4. (Left) PMT single photoelectron spectrum and its various components. The pedestal (red) corresponds to the noise distribution. The Gaussians for the SPE and multi-PE peaks are shown in blue. The exponential function (yellow) is included to account for the under-amplified photoelectron signals and improves the overall fit (green). (Right) Distribution of the measured gains at 1500 V for the 248 selected tubes (blue) and all the 321 tested PMTs (red). An average value of 5.3×10^6 with a spread of 2.1×10^6 is computed for the selected group and a similar value is found for all PMTs: 5.4×10^6 with a spread of 2.1×10^6 .

The baseline noise from the electronics results in a pedestal in the SPE spectrum described by a Gaussian of amplitude A_0 , mean μ_0 and width σ_0 . The pedestal is followed by the SPE peak with Gaussian parameters A_1 , μ_1 and σ_1 . Given the single photon intensity of the light source, higher PE contributions follow Poissonian statistics and their Gaussian parameters are thus dependent on the SPE values as shown in the total fit function that follows:

$$A_0 \exp\left(-\frac{(x - \mu_0)^2}{2\sigma_0^2}\right) + \sum_{i=1}^N A_i \exp\left(-\frac{(x - i\mu_1)^2}{2i\sigma_1^2}\right) + B \exp(-x\tau). \quad (1)$$

The exponential function is included to account for the under-amplified photoelectron signals and its addition improves the overall fit at the valley between the pedestal and single photoelectron peak (as in [13] and [17]). The gain is computed as $g = \frac{\mu_1}{e}$, with e being the elemental charge.

Figure 4 (right) shows the distribution of gains derived from the SPE spectra at 1500 V (for simplicity, the absolute HV value is stated through this article, although the PMT bias voltage is

always negative). The average gain for all PMTs at 1500 V is 5.4×10^6 with a standard deviation of 2.1×10^6 , while the value for those selected for XENON1T is 5.3×10^6 and a spread of 2.1×10^6 .

The gain at room temperature has been measured for every PMT at 8 different voltages between 1320 V and 1680 V with an LED illumination at single-photon intensity. The scan allows to determine the gain as a function of HV for each PMT, fitting the data with a power law curve. In XENON1T the operating gain for each PMT, and hence the voltage, will be determined based on the separation of the signal from the noise pedestal. The optimal gain selection will consider such parameters as the SPE resolution and peak-to-valley ratio, described in the following section.

3.3 Single photoelectron resolution and peak-to-valley ratio

The SPE peak resolution is defined as $R = \frac{\sigma_1}{\mu_1}$, where σ_1 and μ_1 are the standard deviation and the mean of the Gaussian function describing the SPE peak (see equation 1). In turn, the peak-to-valley ratio is calculated by dividing the maximum height of the SPE peak and the minimum value of the valley between the peak and the noise pedestal. It depends on the characteristics of the PMT as well as the specific noise conditions of the experiment.

Both parameters can be extracted from the measured spectra as the one shown in figure 4 (left) and allow to quantify the resolution and the separation power between the noise pedestal and the single-photon response. In general, a better separation of the signal from the noise improves the energy threshold of a detector. Thus, an optimization of the two parameters as a function of gain is crucial for an optimal performance of XENON1T.

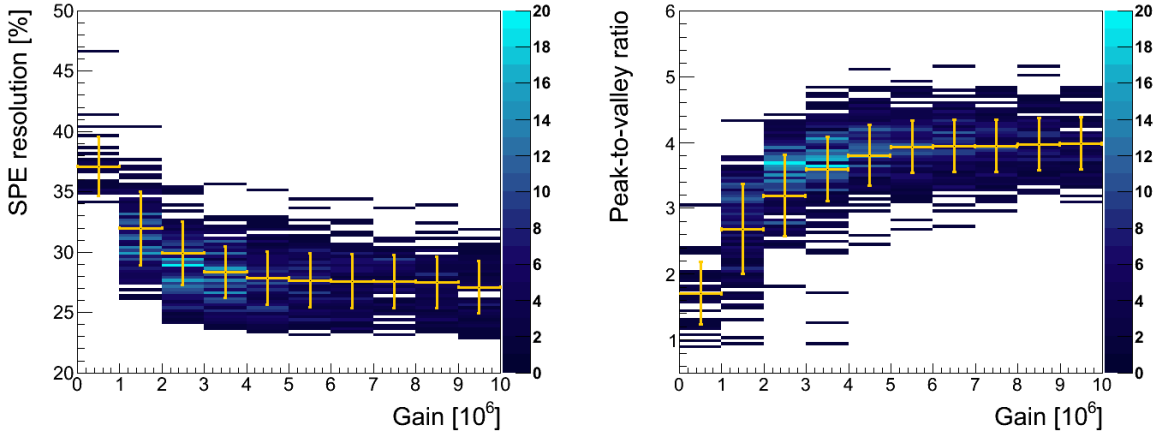


Figure 5. (Left) Single photoelectron resolution as a function of gain for the XENON1T selected PMTs. (Right) Peak-to-valley ratio as a function of gain. The color coded scale displays the number of PMTs. For each bin the average resolution and standard deviation are shown by the yellow markers.

Figure 5 (left) shows the SPE resolution as a function of gain for the XENON1T PMTs. The yellow markers indicate the mean for binned values of the gain. It can be seen that the resolution of approximately 27 % does not improve significantly for gains above 3×10^6 . Figure 5 (right) shows the data for the peak-to-valley ratio. For gains larger than 3×10^6 the values remain approximately constant at around 4. These results suggest an optimal operation of the PMTs at gains between

$(2 - 3) \times 10^6$, given that low gains reduce signal saturation in the read-out electronics and low bias voltages minimize the stress on the PMTs during long-term operation.

3.4 Transit time measurement

The timing performance of a PMT is characterized by the transit time (TT), measured as the time difference between the LED trigger (emission of the photon) and the arrival of the electron avalanche at the anode. This is relevant since a signal in XENON1T is generally observed by more than one PMT. Hence, the transit time spread (TTS) defines the time window for coincident events between PMTs. A smaller time window allows to reduce possible random coincidences.

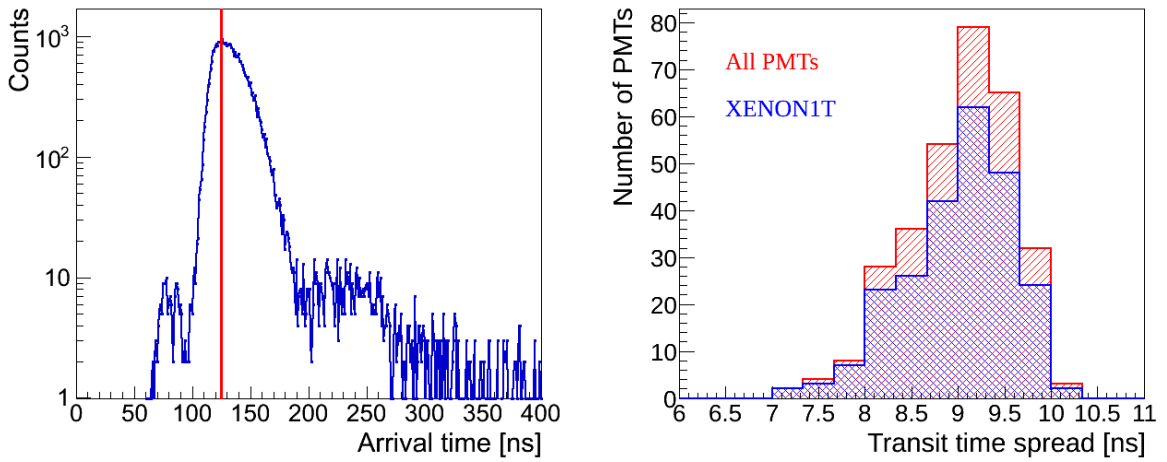


Figure 6. (Left) Transit time response for a single PMT with the mean arrival time of 125 ns (red line). (Right) Distribution of the transit time spread, defined as the FWHM of the main peak, for all (red) and selected (blue) tubes.

The TT spectrum of a single PMT is shown in figure 6 (left). The arrival of the electron avalanche at the anode is approximately 125 ns after the LED trigger. This TT also includes the time delay from the electronics of the setup. The TT estimated by Hamamatsu for the photoelectron only, between the photocathode and the first dynode, is 46 ns. The faster signals seen before the main peak are likely caused by photons passing through the photocathode and interacting directly with the first dynode. The events occurring after the main peak can be caused by photoelectrons backscattering off the first dynode [18].

The TTS is defined as the FWHM of the main peak. This spread is a result of the different trajectories of photoelectrons through the PMT according to their initial positions and velocities at the photocathode. The TTS distribution for all PMTs is shown in figure 6 (right) with a mean of (9.2 ± 1.3) ns. If this spread is convoluted with the 1.4 ns pulse width of the LED, the TTS for the tubes alone is reduced to (9.1 ± 1.3) ns, showing that the LED pulse width has a negligible impact on the measurements. These results are in agreement with the TTS of 9 ns reported by Hamamatsu.

3.5 Dark count rates

The dark count (DC) rate of a PMT describes the number of signals per second above a given threshold in the absence of a light source. These signals are produced mainly by thermal electrons emitted when the PMT is powered at a certain voltage. At cryogenic temperatures, a non-thermal DC remnant is present caused, in part, by electron field emission. A low dark count rate in XENON1T is important to reduce accidental coincidences between PMTs. These random coincidences can imitate the detection of scintillation signals in the detector and, hence, contribute to the background during a dark matter search.

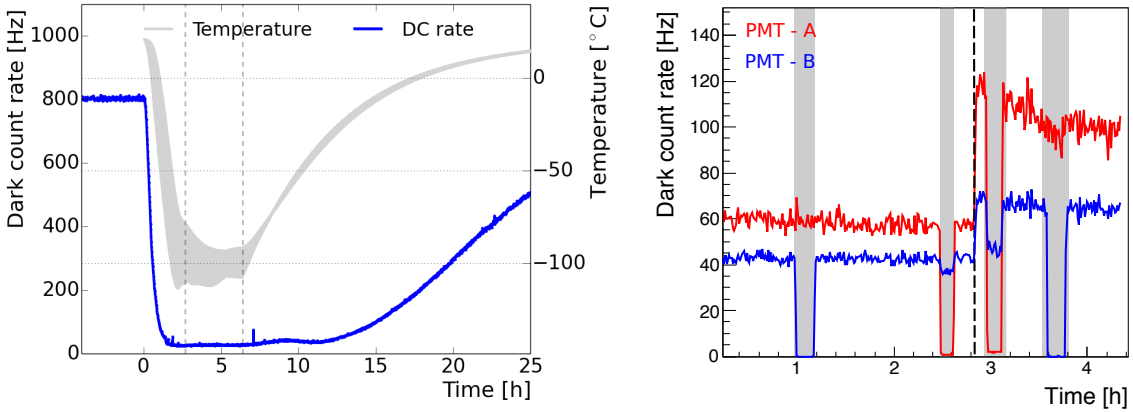


Figure 7. (Left) Dark count rate evolution during cool down (blue curve). The shaded grey area indicates the temperature range between the lower PMT array (position 3 in figure 1) and the upper PMTs (position 6). The vertical dashed lines indicate the time period of stable temperature. (Right) During stable temperature operation, tests for light emission are performed by measuring changes in the DC rates (see text).

Figure 7 (left) shows an example of a DC rate measurement during a cooling cycle in the setup described in 2.1. The time evolution of the dark count rate and its dependence on temperature is shown. The measurement starts at room temperature, with the DC rate dropping sharply at $T = 0$, indicating the beginning of the cool down at an average rate of 1.5 K/min. Already at around -30°C the DC rate reaches values close to its minimum. During the cooling process, the DC rate can show some instabilities, possibly due to small discharges inside the tube. After approximately 2.5 hours the temperature has decreased and stabilized at around -100°C , where the DC rate remains at an approximately constant value. The performance of the tube is evaluated during the stable period until the cooling of the chamber is stopped. As the system heats up, the DC rate of the PMT also rises to its previous value at room temperature. A minimum of 2 cool downs are performed for every PMT, during which different settings of the bias voltage are used: 1500 V, 1680 V and the voltage corresponding to a gain of 3×10^6 .

Figure 7 (right) shows the dark count rates of two PMTs facing each other during the period of stable temperature at -100°C . To the left of the dashed line, the PMTs are operated at a gain of 3×10^6 , corresponding to voltages between (1300 – 1500) V. To the right of the line, the voltages have been increased to 1680 V. The grey areas indicate time periods where one of the two PMTs was switched off to study its level of light emission. It can be seen that PMT-A emits light given

that, when it is turned off, the opposite PMT shows a reduced dark count rate. Furthermore, the reduction is larger at 1680 V ($\Delta = 25$ Hz) than at lower voltages ($\Delta = 10$ Hz), indicating a correlation with the bias voltage. A detailed study of this light emission effect is presented in section 4.

Figure 8 shows the histograms of the obtained dark count rates for all tested (red) and the XENON1T PMTs (blue) at an equalized gain of 3.0×10^6 at room temperature (left) and at -100°C (right).

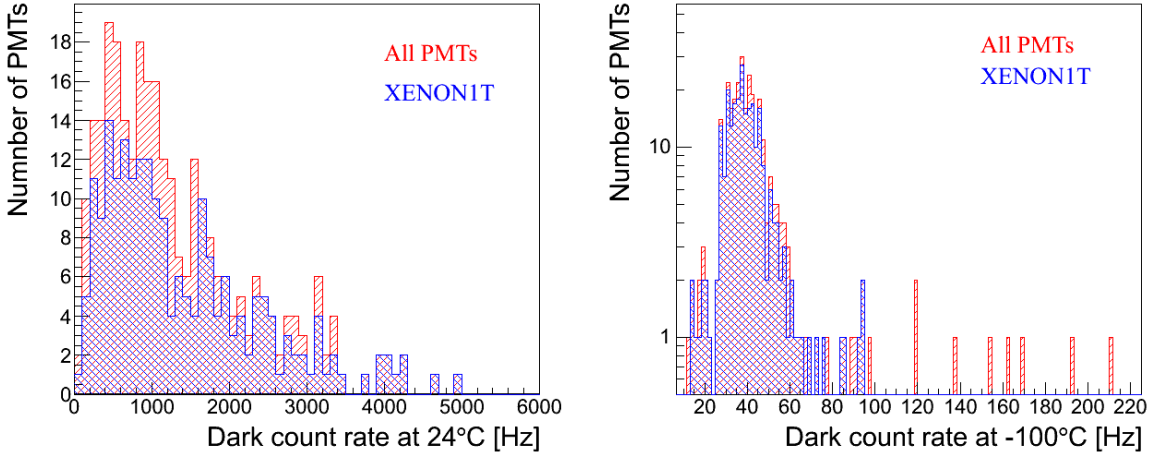


Figure 8. (Left) Distribution of the dark count rates at an equalized gain of 3×10^6 at room temperature. (Right) Dark count rates at -100°C . The red histograms show the data for all tested PMTs, while the blue histograms correspond to the PMTs selected for XENON1T.

The average dark count rate shows a value of 1348 Hz (1400 Hz) at room temperature for all (XENON1T) tubes with a large standard deviation of around 988 Hz (1025 Hz). However, after cooling the tubes to -100°C , the mean DC rate reduces to 44 Hz (40 Hz) with a smaller standard deviation of 24 Hz (13 Hz) for all 321 tested (selected) tubes. In the right figure, the red histogram shows a population of PMTs with rates above 100 Hz which have been rejected due to light emission or an unstable dark count rate. It is important to mention that the measured dark count rates depend on the pulse height threshold at which the counter trigger is set. For these measurements a threshold at $\sim \frac{1}{4}$ PE has been used. The rates also depend on the shielding of the test setup and the distance between the opposing PMT structures. A larger distance between the PMT arrays increases the measured values and spread of the DC rates, likely due to an increased solid angle to observe Cherenkov light or scintillation (390 nm wavelength photons [19]) in the N_2 gas from ionizing radiation such as cosmic rays and α particles.

4 Detection of light emitting PMTs

During the DC rate measurements described in section 3.5, some cases of light emission from the phototubes have been identified. This behaviour is problematic for rare event searches, such as dark matter detection, since it may produce coincident pulses in the detector that can be interpreted as a scintillation signal. If the level of light emission is too large, those accidental coincidences

might create an irreducible background to the dark matter search and could significantly limit the sensitivity of the detector. The quantification of such light emission is not straightforward since it depends strongly on the setup and ambient conditions. However, a qualitative study has been made by observing a change in the dark count rates of either the light emitting PMT itself or of the PMT facing it. The absolute change of the dark count rate will depend on the amount of collected light, which, in turn, depends on the solid angle between the opposing tubes. This method is thus not an absolute measurement of the total light emission, and the quantitative results may vary in XENON1T.

Two main categories of light emission have been observed in the extensive testing campaign described here. In some cases, the tube emits a large amount of light within a period of a few seconds. This so-called “flash” is observed by the tube itself and the PMTs operated on the opposite array, increasing the measured rates. Due to the exposure of the PMT cathode to the light from this event, the rates can take from several minutes up to a few hours to decrease to the previous levels. The microscopic processes causing this spontaneous and strong light emission are not completely understood, but, given their rare occurrence (in only $\sim 1\%$ of all PMTs tested) and straight-forward identification, tubes in which only one such event has been observed were not rejected.

The second type, denominated “micro light emission”, is harder to observe since it is only detectable by a small change of the dark count rate of the opposing PMT, as explained previously in figure 7. The level of micro light emission is defined by the difference of the average dark count rate induced by the tested PMT which is turned on and off. This method allows to quantify the observed light emission for several HV values and the functional dependence on the HV can be derived, as shown in figure 9 (left). Results are presented for measurements at room temperature and at $-100\text{ }^\circ\text{C}$ for several PMTs.

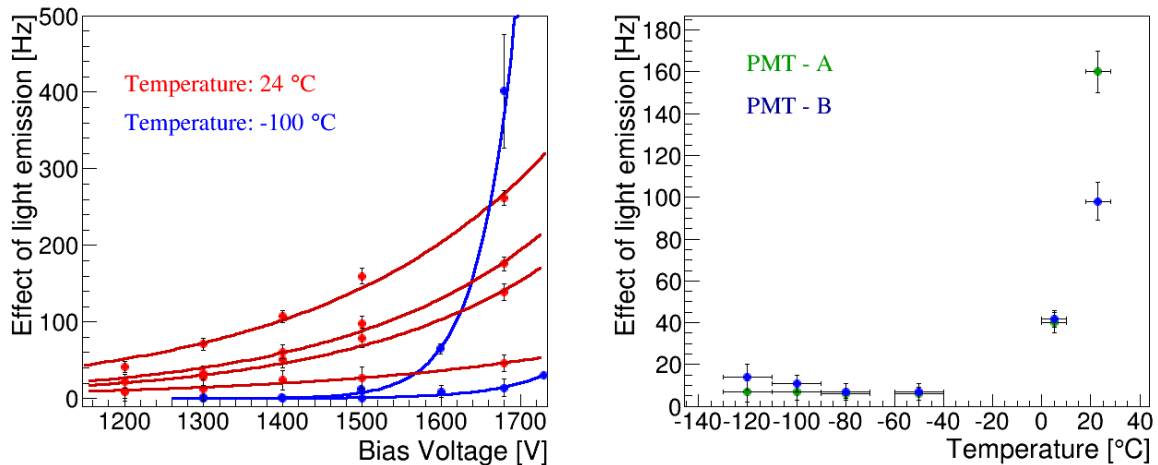


Figure 9. (Left) Change of the dark count rate due to a light emitting PMT with respect to the applied bias voltage. It can be seen that the amount of emitted light is dependent on the HV, and if the tube is operated at sufficient low bias voltages, light emission is not observable with this method. The effect of light emission for different PMTs at room temperature is indicated by the red lines, while the measurements at $-100\text{ }^\circ\text{C}$ are shown in blue. (Right) Correlation between the effect of light emission on two PMTs and different operation temperatures at a constant bias voltage of 1500 V.

The effect of light emission decreases with lower bias voltages and is larger at higher temperatures while it is typically suppressed at cryogenic temperatures. This method, however, might not be sensitive enough to detect a small level of micro light emission at low bias voltages. Figure 9 right shows the temperature dependence of the effect at 1500 V. This suggests that if a PMT shows micro light emission, it scales in general with the dark count rate of the PMT. The temperature dependence of the dark count rate can also be observed in the left plot in figure 7. Light emission has been measured in a total of 53 PMTs. These have been returned to Hamamatsu and replaced. Other studies of the R11410 PMT have also shown light emission due to processes within the tube [20].

5 Measurements in gaseous and liquid xenon

After the PMTs have been tested at room temperature and cooled down in a nitrogen environment, a subset has been selected for testing in both gaseous and liquid xenon. This selection includes PMTs with unstable behaviour during the general testing described earlier or hints of possible leaks, as will be discussed in section 6.2.

As described in section 2.2, the xenon testing facility allows 5 tubes to be operated simultaneously. The measurements are performed over a period ranging from a couple of weeks to several months. The cooling of the system is achieved by filling gaseous xenon (GXe) into the chamber over several steps. In the first step, after reaching a vacuum pressure below 2×10^{-5} mbar, around 0.1 kg of xenon gas is introduced into the chamber, raising the absolute pressure to 1.8 bar. As the PTR cools the system and the pressure decreases close to 1.4 bar, more xenon is filled to increase the cooling rate. The set point around -100 °C is reached in approximately 24 hours, corresponding to an average cooling rate below 0.1 °C/min. For measurements in liquid, 2.8 kg of xenon are filled to cover the PMT body. Figure 10 shows an example of the cooling cycle for a PMT in xenon. Several such cool downs are performed for each PMT to test the stability and resistance to thermal cycling.

5.1 Dark count rate stability

The xenon testing facility allows for long-term measurements of PMT properties given that it operates at very stable conditions for long periods of time. During cryogenic operation, the temperature in the cryostat can be kept stable within 0.2 °C during a day. The changes over a month of operation are no larger than 2 °C. The pressure, in turn, varies within 0.03 bar in a day and up to 0.07 bar within a month.

The blue curve in figure 10 shows an example of the dark count rate of an R11410-21 PMT at 1500 V during cool down. The average dark count rate of 30 PMTs tested at -100 °C in GXe was measured to be (46 ± 4) Hz over several weeks. This represents a stability of around 10 % for the dark count rate of the XENON1T PMTs at cryogenic temperatures. The average DC rate in cold GXe is in agreement with the cold test results from section 3.5, in which the mean rate was (44 ± 23) Hz. When filling the chamber with LXe, the PMT dark count rate increases from tens of hertz to a few hundred hertz. This is due to scintillation light produced by interactions of cosmic and ambient radiation in the liquid medium.

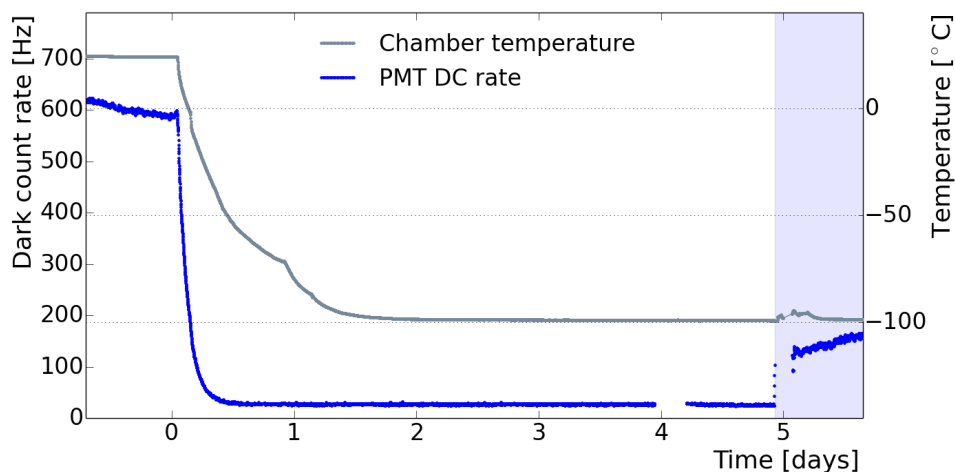


Figure 10. Evolution of the dark count rate of a PMT during operation in gaseous and liquid xenon. The gray line indicates the temperature of the inner chamber during cool down. The rate (blue line) decreases from hundreds of Hz at room temperature to an average of 28 Hz when operated in the gas phase, at around -100°C , remaining stable within 2 Hz. The blue shaded area indicates a filling of liquid xenon, after which the rate increases to about 200 Hz due to the scintillation light in the liquid phase.

5.2 Gain evolution

The gain of the PMTs has been measured at cryogenic temperatures both in gas and liquid xenon. Figure 11 shows the gain evolution of a PMT during cool down from room temperature to -100°C in a xenon environment.

When cooled and maintained in GXe, the gain increases and settles at a value higher than at room temperature. This effect is explained by the decrease in electric resistance of the PMT components, voltage divider and signal cables, which results in a higher charge output. The same effect has been measured in the nitrogen cooling setup. On the other hand, when covered by LXe, a decrease of the PMT gain is observed. The direct contact with the LXe seems to have an effect on the PMTs, although the exact reason for the gain decrease is not fully understood. The same observation has been reported in [7].

For the PMTs tested in xenon, the average increase of the gain between room temperature and GXe at -100°C has been measured to be around 7 %, while an average decrease of 3 % is observed during operation in LXe with respect to the values in cold GXe.

6 Study of afterpulses and leak identification

A detailed study of the afterpulses in the R11410-21 phototube has been performed following the methods introduced in [7]. The results presented here focus on the evolution of the afterpulse rates and spectra after operation of the phototubes in cold Xe. The methods for the identification of ions within a PMT are detailed and implemented for the diagnosis of leaks which can appear when cooling down the tubes.

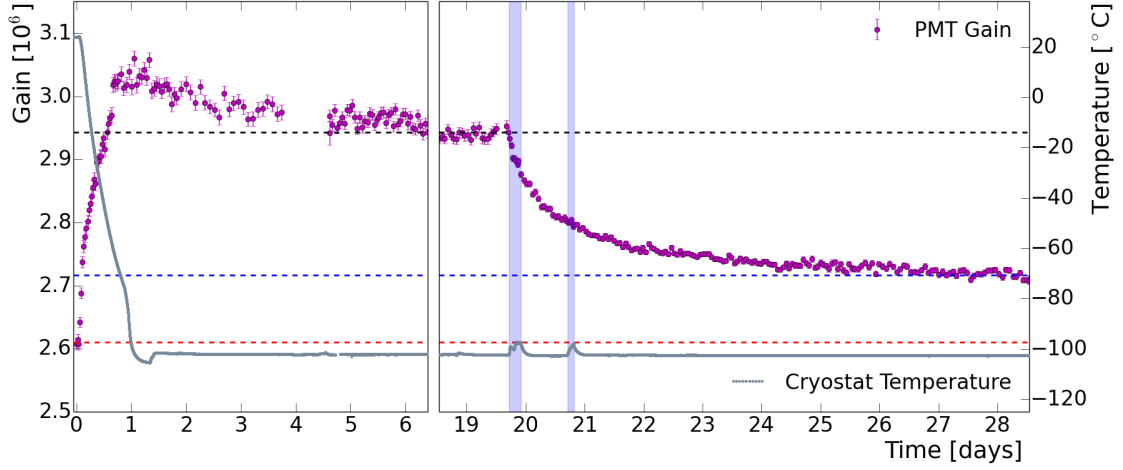


Figure 11. PMT gain evolution during cool down in gas xenon (first 20 days) and liquid xenon (filling on days 20 and 21, indicated by the blue shaded areas). An increase of around 12 % in the gain is measured between room temperature and -100°C gaseous xenon. After the filling of liquid xenon, a decrease of around 7 % is observed in the gain with respect to the value in the gas phase.

6.1 Ion identification through afterpulse timing

Residual gas molecules in the PMT vacuum comprise one of the sources for afterpulsing. In its trajectory from the photocathode to the first dynode, a photoelectron may ionize a molecule, which in turn drifts to the photocathode and generates an afterpulse. A specific ion can be identified by the time delay between the afterpulse and the main pulse that generated it. An ion generated at the position s_0 between the focusing grid (located at 0) and the PMT photocathode (distance L) will have the following travel time t :

$$t = \int_{s_0}^L \frac{1}{v(s)} ds = \sqrt{\frac{m}{2q}} \int_{s_0}^L [V(s_0) - V(s)]^{-1/2} ds, \quad (2)$$

where the velocity $v(s)$ as a function of position has been determined with the Lorentz force equation in an electric field. The mass and charge of the ion are m and q , respectively, and $V(s)$ is the electric potential as a function of position.

At first approximation, the field between the photocathode and focusing grid may be considered that of a parallel plate capacitor. However, for PMTs such as the 3-inch R11410 models, the field lines converge towards the focusing grid, as seen in the field simulation of figure 12 (left). Thus, a better approximation is obtained with a quadratic potential of the form: $V(s) = V_0 \left(1 - \frac{s}{L}\right)^2$ (see also [21]). The position of ionization will be considered to be close to the focusing grid, $s_0 = 0$. This is a valid assumption given that the electron energy is lowest at the photocathode and greatest at the grid, increasing the probability of ionization. Hence $V(s_0) = V_0$.

Equation 2 can then be solved as:

$$t = \sqrt{\frac{m}{2q}} \frac{2L}{\sqrt{V_0}} \arctan\left(\frac{\sqrt{s}}{\sqrt{2L-s}}\right)\Big|_0^L = \frac{\pi}{4} \sqrt{\frac{2m}{qV_0}} L. \quad (3)$$

Ion	M/Q	Afterpulse Time [μs]		
		Measured	Calculated	Simulated
H ⁺	1	0.28 \pm 0.02	0.26 \pm 0.01	0.27 \pm 0.01
H ₂ ⁺	2	0.39 \pm 0.02	0.37 \pm 0.01	0.38 \pm 0.01
He ⁺	4	0.52 \pm 0.02	0.52 \pm 0.01	0.52 \pm 0.01
CH ₄ ⁺	16	1.01 \pm 0.03	1.03 \pm 0.02	1.02 \pm 0.02
Ne ⁺	20	1.13 \pm 0.03	1.16 \pm 0.03	1.14 \pm 0.02
N ₂ ⁺	28	1.33 \pm 0.03	1.37 \pm 0.03	1.33 \pm 0.03
Ar ⁺	40	1.58 \pm 0.04	1.63 \pm 0.04	1.57 \pm 0.03
Xe ⁺⁺	65	2.02 \pm 0.05	2.08 \pm 0.05	2.02 \pm 0.04
Xe ⁺	131	2.85 \pm 0.07	2.96 \pm 0.07	2.80 \pm 0.06

Table 1. Several residual molecules in the PMT have been identified as generators of afterpulses. M/Q corresponds to the mass-to-charge ratio in nucleons over units of charge. The time delay measured by experiment is compared to the calculated value from equation 4 and the result from simulations. The experimental errors correspond to the spread of each peak. The calculated errors are propagated from the measurement uncertainty of the distance between photocathode and focusing grid, as well as the value of the voltage divider resistors. To quantify the uncertainty in the simulations, the grid-to-dynode distance and resistor values have been varied, and the distribution spread for each simulated ion has been taken into account.

This differs from the result for a parallel plate model by a factor $\pi/4$. Equation 3 can be simplified by introducing the proton mass and charge, substituting $1C = (\text{kg m}^2)/(\text{V s}^2)$ and rewriting the terms in units of cm and μs :

$$t = \left(1.134 \frac{\text{V}^{1/2} \mu\text{s}}{\text{cm}} \right) \sqrt{\frac{L^2 M}{V_0 Q}}, \quad (4)$$

with V_0 in volts, L in cm and t in μs . M/Q is the mass-to-charge ratio of the ion, set in number-of-nucleons/units-of-charge and is thus dimensionless. In the case of the R11410-21 tube, $L = 4.1$ cm. When operated at 1500 V, using the XENON1T voltage divider, the potential difference corresponds to $V_0 = 323.4$ V. Table 1 shows the identified ions from afterpulses in the tubes, comparing the experimental measured times, the calculated times from equation 4 and the times obtained from the simulations described next.

For simulations of the electric field and transport of electrons and ions, a model of the PMT has been developed using the COMSOL Multiphysics[®] software [22]. The dimensions have been taken from direct measurement of the elements in an opened tube. In particular, the focusing grid and dynodes have been reproduced in detail. Figure 12 (left) shows the simulation of the electric field in the PMT. The drift of electrons from the photocathode to the first dynode has been simulated. The average transit time was measured to be (45.4 ± 1.8) ns, with a collection efficiency of 95 %. These values are in agreement with those reported by Hamamatsu (see section 3.4), where the transit time is (46 ± 9) ns and the photoelectron collection efficiency is around 90 % [6]. Several of the ions experimentally identified to cause afterpulses have been simulated and their corresponding drift times are presented in table 1. The experimental, calculated and simulated results differ on average by about 3 %, being in good agreement when taking into account the uncertainties de-

scribed in table 1. This suggests a high accuracy for ion identification. The comparison is also shown in figure 12 (right). The slight deviations between the calculated drift times for Xe ions with respect to the simulated and experimental values indicate that the quadratic potential implemented in section 6.1 is a good approximation but not an exact description of the complex electric field in the PMT, shown in figure 12 (left).

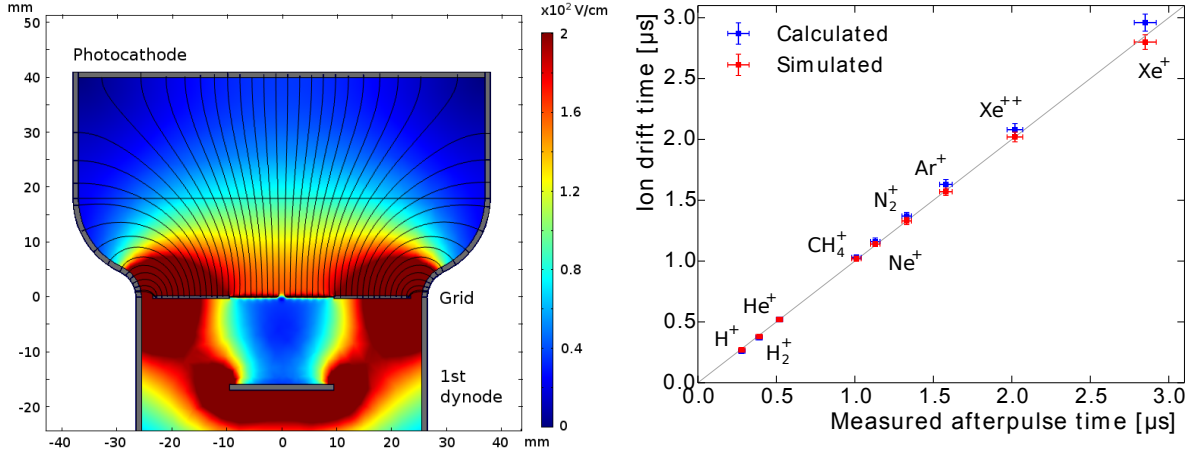


Figure 12. (Left) Simulation of the PMT electric field using COMSOL Multiphysics[®]. The color scale indicates the field strength in V/cm. Electron and ion transport have been simulated in the generated field, allowing to estimate their transit times. (Right) Comparison of the calculated (blue) and simulated (red) ion drift times with respect to the experimental afterpulse results. Values taken from table 1. The diagonal line indicates a one-to-one relation, for reference.

6.2 Afterpulse analysis and leak diagnosis

The afterpulses generated by ions are characterized by amplitudes of several photoelectrons and appearance at specific times, determined by the mass and charge of the ion, as discussed before. Such afterpulses have been classified in the group A3 of figure 13 (left). The figure shows the size of the afterpulses, normalized to that of a single photoelectron on the y axis, while the x axis corresponds to the afterpulse transit time. Other groups of afterpulses have also been identified according to their characteristics and origin: A1– Pulses with a very short time delay (several tens of nanoseconds) and amplitudes around 1 PE, possibly generated by secondary electrons scattering off the first dynode which backtrack and successively strike again the first dynode. A2– Pulses with a time delay of up to several microseconds and amplitudes around 1 PE. This population is generated by dark pulses and single electrons of unclear origin.

Afterpulse measurements have been performed for the PMTs at room temperature and in LXe. Figure 13 (right) shows a comparison of the afterpulse spectra for a PMT in each environment, according to the afterpulse groups defined in the left plot. An analysis of the afterpulse rates has been performed by recording several million single photon triggers (from dark pulses) and the pulses that follow within a $4\ \mu\text{s}$ window. The afterpulse rate is given as a percentage of the total SPE trigger signals. The mean afterpulse rate at room temperature for 44 PMTs is $(1.4 \pm 1.2)\%$. The ions producing the highest rates are He^+ $(0.02 \pm 0.01)\%$, CH_4^+ $(0.07 \pm 0.03)\%$ and Ar^+ $(0.08 \pm 0.07)\%$.

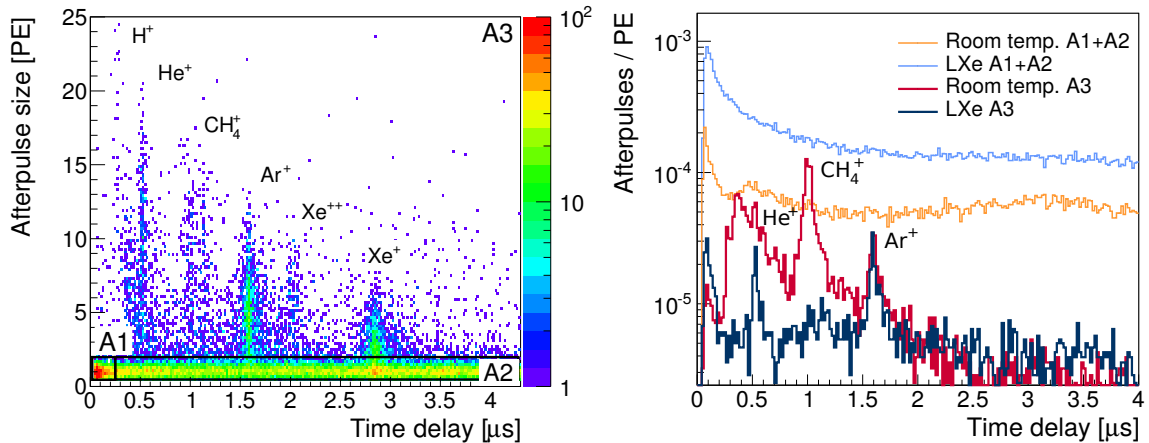


Figure 13. (Left) Afterpulse size and time delay for a PMT at room temperature after operation in LXe. The afterpulses are classified into groups A1, A2 and A3, according to their origin. The group A3 corresponds to afterpulses generated by ions of residual gas molecules in the PMT vacuum, which have been identified according to the analysis described in section 6.1. (Right) Comparison of afterpulses in A1+A2 and in A3 for a PMT at room temperature and in LXe.

Afterpulses [%]:	Total	A1	A2	He ⁺	CH ₄ ⁺	Ar ⁺
Room temp.	1.4 ± 1.2	0.11 ± 0.05	0.9 ± 1.1	0.02 ± 0.01	0.07 ± 0.03	0.08 ± 0.07
LXe	8.6 ± 2.2	1.8 ± 0.5	6.4 ± 1.7	0.02 ± 0.01	0.02 ± 0.01	0.08 ± 0.02

Table 2. Afterpulse rates given as a percentage of the total SPE trigger pulses. A comparison is made between the measurements at room temperature and in LXe. The errors are computed statistically as mean absolute deviations. The rate increase in LXe is due to the A2 afterpulses from single photoelectrons distributed homogeneously in time, whereas the afterpulses from identified ions remain on average the same or decrease. Ions not shown in the table have an average rate below 0.02 % of the total triggers.

All other ions show rates below 0.02 % of the total trigger signals. The afterpulse rates were also recorded in LXe for 11 of those PMTs, in which case the mean afterpulse rate increased to (8.6 ± 2.2) %. The main increase was seen in the A2 group consisting of afterpulses with SPE amplitudes spread out homogeneously over several microseconds. These afterpulses may be caused by photons from the micro light emission described in section 4. On the other hand, the average contributions of He⁺ and Ar⁺ remain unchanged, whereas the mean CH₄⁺ rate decreased to (0.02 ± 0.01) %. The reason for this is unclear, but may be related to the adhesion of the different compounds to the PMT surfaces. The results are summarized in table 2.

The ions which most contribute to afterpulsing have been labeled in the example spectra of figure 13. It can be observed that the mean size of the afterpulses decreases with the mass of the ion. Figure 14 (left) shows the afterpulse size distribution for selected ions. Heavier ions like Xe⁺ produce afterpulses with a mean around 2 PE, while lighter ions like H⁺ produce larger afterpulses of around 18 PE with a larger spread. Figure 14 (right) shows the distribution of the mean CH₄⁺ afterpulse size in PE compared to the QE of each PMT. The Pearson correlation coefficient is found to be 0.74, indicating a direct correlation between the observables. This shows that a photocathode

with a higher electron yield from photons also generates more electrons from impinging ions, as could be expected. As a result, the measurements of afterpulse size in photoelectrons can give an insight into the quantum efficiency of a PMT.

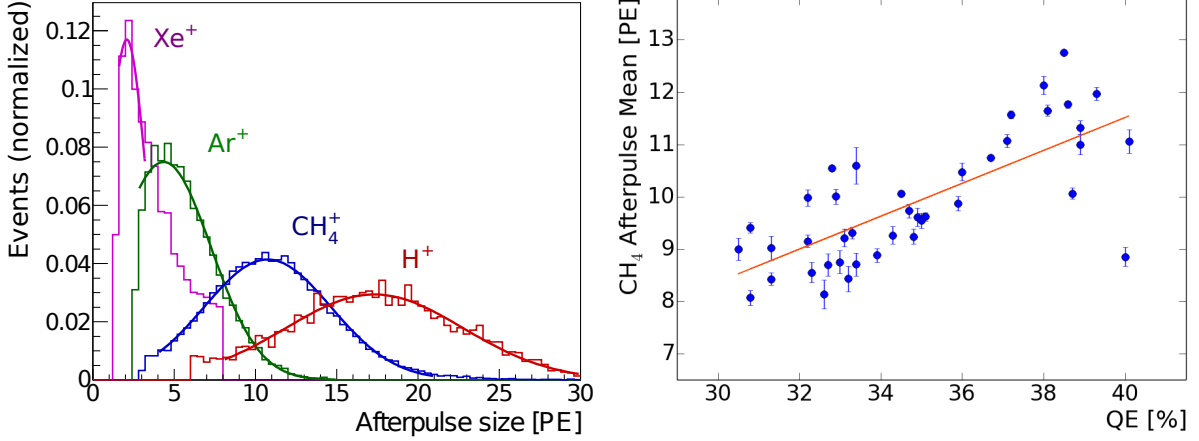


Figure 14. (Left) Afterpulse size distributions for selected ions. Heavier ions like Xe^+ produce smaller afterpulses, while lighter ions like H^+ , generate larger afterpulses. (Right) Distribution of the mean CH_4^+ afterpulse size compared to the QE of each PMT. A linear fit is applied to the data (orange line) and the Pearson correlation coefficient is found to be 0.74. This indicates a direct correlation between the observables, meaning that the measured number of photoelectrons in afterpulses gives an insight into the quantum efficiency of a PMT.

This afterpulse analysis also allows to diagnose the presence of leaks in faulty PMTs during cool down. Out of the 44 PMTs tested in LXe, 8 presented the appearance of Xe afterpulses. Figure 15 shows the spectra of the A3 group afterpulses for the same PMT before and after cool down. A clear rise of afterpulses around $2.8\mu\text{s}$ is observed. For this PMT the Xe^+ afterpulse rate increased to 0.04 %, while the Xe^+ rates for other PMTs with a leak increased to as much as 0.98 %. These PMTs have been returned to the production company, where the presence of Xe in the tubes has been confirmed and the PMTs have been replaced.

It is important to remark that many of the PMTs tested in Xe were pre-selected from the observation of an N_2 afterpulse increase after their first cryogenic tests or other issues such as unstable DC rates or flashing (described in section 4). Thus, the statistics for the appearance of Xe leaks is not representative of the full set of PMTs installed in XENON1T, of which the majority showed no such issues during the tests described here.

7 Summary

In this article we report on the extensive testing campaign of 321 R11410-21 photomultiplier tubes, out of which 248 have been selected for long-term operation in the XENON1T experiment. The evaluation of the tubes is based on the dark count rate, SPE response, transit time spread, quantum efficiency, and level of light emission. Detailed measurements have been performed on a subset of PMTs in gaseous and liquid xenon. The evolution of the dark count rate and gain have been studied,

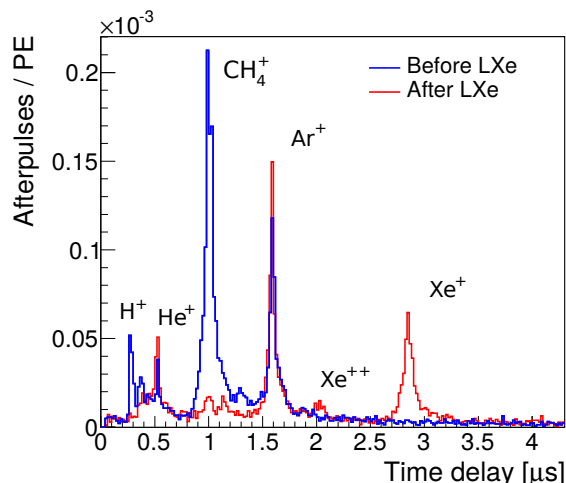


Figure 15. Example afterpulse spectra taken before (blue) and after (red) operation of a faulty PMT in liquid xenon. The appearance of a xenon peak at $2.8\mu s$ is a clear indicator of a leak in the PMT. The decrease of CH_4^+ has been observed in all PMTs after operation at cryogenic temperatures, as presented in table 2.

showing the viability to operate the tubes long-term in a dark matter experiment. The identification of residual gas molecules within the PMTs through the study of afterpulses has been described, proving to be a useful method for diagnosis of the PMT vacuum quality and leak identification.

A total of 73 tubes, 22 % of the amount tested, have been rejected and thus excluded for use in XENON1T. Out of these, 12 tubes have been rejected due to an elevated or unstable dark count rate, either at cryogenic or room temperature. A larger amount, 53 in total, presented light emission. Out of the 44 PMTs tested in LXe, 8 were identified to show afterpulses from xenon ions, indicating a leak in the tube and thus being unsuited for long-term operation. It must be noted that the leak statistics is not representative of the whole set, since most PMTs tested in LXe were selected for their unstable performance during previous tests or suspicion of a leak after operation in nitrogen gas at $-100^\circ C$.

The selected 248 PMTs have an average quantum efficiency of $(34 \pm 3)\%$ and show a low average dark count rate of (40 ± 13) Hz at $-100^\circ C$. At a gain between $(2 - 3) \times 10^6$ the peak-to-valley ratio ranges from 2.5 to 4.5, proving the large signal to noise separation of this tube. During their operation in XENON1T, the evolution of the gain and dark count rates will be monitored for all PMTs. The methods presented here will also allow to identify the appearance of light emission or leaks in the tubes throughout the course of the experiment.

Acknowledgements

We thank Hamamatsu for the fruitful collaboration and production of the PMTs used in these studies and in XENON1T. We also thank Andreas James, Daniel Florin and Martin Auger at UZH, and Reinhard Hofacker at MPIK, for their technical support. We gratefully acknowledge the support from the Swiss National Science Foundation, the European Union FP7 ITN INVISIBLES (Marie Curie Actions, PITN- GA-2011- 289442), the Max-Planck society and the DFG research train-

ing group 'Particle physics beyond the standard model'. We acknowledge the XENON Bologna colleagues for providing a few PMTs.

References

- [1] Teresa Marrodán Undagoitia and Ludwig Rauch. Dark matter direct-detection experiments. *J. Phys.*, G43(1):013001, 2016.
- [2] Laura Baudis. Dark matter detection. *J. Phys.*, G43(4):044001, 2016.
- [3] E. Aprile et al. Physics reach of the XENON1T dark matter experiment. *JCAP*, 1604(04):027, 2016.
- [4] O. Cheshnovsky, B. Raz, and J. Jortner. Temperature dependence of rare gas molecular emission in the vacuum ultraviolet. *Chem. Phys. Lett.*, 15:475, 1972.
- [5] E. Aprile et al. Lowering the radioactivity of the photomultiplier tubes for the XENON1T dark matter experiment. *Eur. Phys. J.*, C75(11):546, 2015.
- [6] K. Lung et al. Characterization of the Hamamatsu R11410-10 3-Inch Photomultiplier Tube for Liquid Xenon Dark Matter Direct Detection Experiments. *Nucl. Instrum. Meth.*, A696:32, 2012.
- [7] L. Baudis, A. Behrens, A. Ferella, A. Kish, T. Marrodán Undagoitia, et al. Performance of the Hamamatsu R11410 Photomultiplier Tube in cryogenic Xenon Environments. *JINST*, 8:P04026, 2013.
- [8] L. Baudis et al. Gator: a low-background counting facility at the Gran Sasso Underground Laboratory. *JINST*, 6:P08010, 2011.
- [9] D. Budjas et al. Highly Sensitive Gamma-Spectrometers of GERDA for Material Screening: Part 2. 2007.
- [10] G. Heusser, M. Laubenstein, and N. Neder. . *Appl. Rad. Isot.*, 2004.
- [11] N. Neder, G. Heusser, and M. Laubenstein. . *Proc. of Intern. Conf. Isotop. Environm.*, 53:19, 2000.
- [12] Annika Behrens. Light Detectors for the XENON100 and XENON1T Dark Matter Search Experiments. PhD thesis, University of Zurich, 2014.
- [13] C. Bauer et al. Qualification Tests of 474 Photomultiplier Tubes for the Inner Detector of the Double Chooz Experiment. *JINST*, 6:P06008, 2011.
- [14] Gaudenz Kessler. Inelastic WIMP-Nucleus Interactions in XENON100 and Cables and Connectors for XENON1T. PhD thesis, University of Zurich, 2016.
- [15] L. Baudis, S. D'Amato, G. Kessler, A. Kish, and J. Wulf. Measurements of the position-dependent photo-detection sensitivity of the Hamamatsu R11410 and R8520 photomultiplier tubes. 2015.
- [16] A. Lyashenko, Tam Nguyen, Adam Snyder, Hanguo Wang, and Katsushi Arisaka. Measurement of the absolute Quantum Efficiency of Hamamatsu model R11410-10 photomultiplier tubes at low temperatures down to liquid xenon boiling point. *JINST*, 9(11):P11021, 2014.
- [17] E. H. Bellamy, G. Bellettini, F. Gervelli, M. Incagli, D. Lucchesi, C. Pagliarone, F. Zetti, Yu. Budagov, I. Chirikov-Zorin, and S. Tokar. Absolute calibration and monitoring of a spectrometric channel using a photomultiplier. *Nucl. Instrum. Meth.*, A339:468–476, 1994.
- [18] Florian Kaether and Conradin Langbrandtner. Transit Time and Charge Correlations of Single Photoelectron Events in R7081 PMTs. *JINST*, 7:P09002, 2012.

- [19] G. Lehaut, S. Salvador, J. M. Fontbonne, F. R. Lecolley, J. Perronnel, and Ch. Vandamme. Scintillation properties of N_2 and CF_4 and performances of a scintillating ionization chamber. Nucl. Instrum. Meth., A797:57–63, 2015.
- [20] D. Yu. Akimov, A. I. Bolozdynya, Yu. V. Efremenko, V. A. Kaplin, A. V. Khromov, Yu. A. Melikyan, and V. V. Sosnovtsev. Observation of light emission from Hamamatsu R11410-20 photomultiplier tubes. Nucl. Instrum. Meth., A794:1, 2015.
- [21] K. J. Ma et al. Time and Amplitude of Afterpulse Measured with a Large Size Photomultiplier Tube. Nucl. Instrum. Meth., A629:93, 2011.
- [22] COMSOL Multiphysics®. The platform for physics-based modeling and simulation. <https://www.comsol.com/comsol-multiphysics>, Accessed July 2016.